

RESEARCH ARTICLE

10.1002/2017JB014476

Key Points:

- Stick-slip recurrence and magnitude are directly linked to RSF parameters—demonstrated via a novel numerical method
- Frictional healing and slip magnitude evolution scale with minimum (or initial) frictional state ($\theta_i = D_c/V$)
- Lag of friction drop evolution with slow (stick) slip is experimentally confirmed

Supporting Information:

- Supporting Information S1

Correspondence to:

K. Im,
kxi123@psu.edu

Citation:

Im, K., Elsworth, D., Marone, C., & Leeman, J. (2017). The impact of frictional healing on stick-slip recurrence interval and stress drop: Implications for earthquake scaling. *Journal of Geophysical Research: Solid Earth*, 122. <https://doi.org/10.1002/2017JB014476>

Received 25 MAY 2017

Accepted 12 NOV 2017

Accepted article online 16 NOV 2017

The Impact of Frictional Healing on Stick-Slip Recurrence Interval and Stress Drop: Implications for Earthquake Scaling

Kyungjae Im^{1,2,3} , Derek Elsworth^{1,2,3,4} , Chris Marone^{2,3,4} , and John Leeman^{2,3,4} 

¹Department of Energy and Mineral Engineering, Pennsylvania State University, University Park, PA, USA, ²EMS Energy Institute, Pennsylvania State University, University Park, PA, USA, ³G3 Center, Pennsylvania State University, University Park, PA, USA, ⁴Department of Geosciences, Pennsylvania State University, University Park, PA, USA

Abstract Interseismic frictional healing is an essential process in the seismic cycle. Observations of both natural and laboratory earthquakes demonstrate that the magnitude of stress drop scales with the logarithm of recurrence time, which is a cornerstone of the rate and state friction (RSF) laws. However, the origin of this log linear behavior and short time “cutoff” for small recurrence intervals remains poorly understood. Here we use RSF laws to demonstrate that the back-projected time of null-healing intrinsically scales with the initial frictional state θ_i . We explore this behavior and its implications for (1) the short-term cutoff time of frictional healing and (2) the connection between healing rates derived from stick-slip sliding versus slide-hold-slide tests. We use a novel, continuous solution of RSF for a one-dimensional spring-slider system with inertia. The numerical solution continuously traces frictional state evolution (and healing) and shows that stick-slip cutoff time also scales with frictional state at the conclusion of the dynamic slip process $\theta_i (=D_c/V_{\text{peak}})$. This numerical investigation on the origins of stick-slip response is verified by comparing laboratory data for a range of peak slip velocities. Slower slip motions yield lesser magnitude of friction drop at a given time due to higher frictional state at the end of each slip event. Our results provide insight on the origin of log linear stick-slip evolution and suggest an approach to estimating the critical slip distance on faults that exhibit gradual accelerations, such as for slow earthquakes.

1. Introduction

Stick-slip frictional instability is a fundamental mechanism contributing to our understanding of the earthquake cycle (Brace & Byerlee, 1966; Scholz, 1998). Periodicity of seismic recurrence and magnitude is widely observed in natural earthquake events (e.g., Nadeau & Johnson, 1998; Rubinstein et al., 2012; Schwartz & Coppersmith, 1984), corresponding to general characteristics of laboratory stick-slip observations. Laboratory observations demonstrate that the magnitudes of periodic slip events increase linearly with the logarithm of recurrence time and define a cutoff time where the log linear trend is back-projected to null healing (Beeler et al., 2014; Ben-david, Rubinstein, & Fineberg, 2010; Ikari, Carpenter, & Marone, 2016; Karner & Marone, 2000; Scholz & Engelder, 1976). Interseismic fault healing includes frictional and lithification processes that dictate the trend of slip magnitude (or stress drop) with the logarithm of seismic recurrence interval (Mclaskey et al., 2012; Scholz, Aviles, & Wesnousky, 1986; Vidale et al., 1994). The slope of the slip magnitude to log time relation can be described in the context of rate and state friction (Beeler, Hickman, & Wong, 2001; Marone, 1998a). However, the cutoff time, an essential element in understanding the evolution of earthquake periodicity and magnitude, remains poorly understood.

Laboratory friction experiments to explore fault healing (slide-hold-slide experiments) demonstrate a log linear trend for waiting time versus peak or “static” friction, with a cutoff time for short aging durations (Dieterich, 1972; Scholz & Engelder, 1976). A variety of micromechanisms have been suggested for the log linear rate of healing, including growth in the real area of contact and plastic deformation between asperities (Baumberger & Caroli, 2006; Beeler, Tullis, & Weeks, 1994; Dieterich & Kilgore, 1994; Ikari, Carpenter, & Marone, 2016; Karner & Marone, 2001; Perfettini & Molinari, 2017; Sleep, 2006; Yasuhara, Marone, & Elsworth, 2005). The same log linear trends are apparent in stick-slip data recorded at different driving rates and thus different slick-slip recurrence times (e.g., Beeler et al., 2014; Karner & Marone, 2000; Mair et al., 2002; Teng-Fong & Yusheng, 1990). The common log linear dependency observed in slide-hold-slide and stick-slip experiments is logically a consequence of the intervention of frictional healing between successive slip events. However,

much work remains to develop a fundamental understanding of healing behavior during the “stick” portion of the stick-slip cycle. For instance, the cutoff time for healing in laboratory experiments is typically on the order of 10^{-1} – 10 s (Marone & Saffer, 2015) while for stick slip this is typically 10^{-3} – 10^{-4} s (Leeman et al., 2014; Scuderi et al., 2015, 2016). One of the purposes of this paper is to illuminate the origin of such discrepancies.

Laboratory cutoff times for frictional healing are known to be dependent on slip velocity (Marone, 1998b), humidity (Frye & Marone, 2002), and temperature (Blanpied et al., 1998; Nakatani & Scholz, 2004; Yasuhara et al., 2005). The cutoff time may be expressed by introducing an initial effective contact lifetime that can be represented by prior slip velocity and a characteristic length of a surface asperity (Bar-sinai et al., 2014; Baumberger & Caroli, 2006; Brechet & Estrin, 1994; Estrin & Brechet, 1996; Nakatani & Scholz, 2006; Rabinowicz, 1951; Rice, Lapusta, & Ranjith, 2001). This velocity dependency is also a consequence of rate and state friction and corresponds with laboratory observations (Marone, 1998b)—suggesting that the healing cutoff behavior is a natural consequence of rate and state frictional response. The velocity dependency of the early-time cutoff for healing may be extended to stick-slip motion as previously discussed (Bar-sinai et al., 2014; Ikari, Carpenter, & Marone, 2016; Nakatani & Scholz, 2006).

The evolution of healing during the interseismic period may be illuminated by numerical simulation of stick-slip motion using rate and state friction laws. However, inertia-controlled stick-slip models have so far required that slow and fast regimes be analyzed separately (He, Wong, & Beeler, 2003; Rice & Tse, 1986; Roy & Marone, 1996). These results are inherently dependent on the preselection of a slip regime, making the analysis of the full spectrum of stick (slow) and slip (fast/inertial) regimes in a common framework difficult.

In the following we demonstrate that the observed cutoff time should intrinsically scale with initial frictional state as defined by rate and state friction. We explore this with the analysis of healing and stick-slip behavior under a common inertial framework for rate and state friction and confirm this response with laboratory observations.

2. Frictional Healing and Rate and State Friction Laws

Rate and state friction (RSF) laws describe the dependence of frictional resistance on slip velocity (V) and an evolving state variable (θ). The most widely used form is (Dieterich, 1979; Ruina, 1983)

$$\mu = \mu_0 + a \ln\left(\frac{V}{V_0}\right) + b \ln\left(\frac{V_0 \theta}{D_c}\right) \quad (1)$$

where μ_0 is a reference friction coefficient corresponding to a reference slip velocity V_0 , D_c is a critical slip distance, and a and b are nondimensional parameters that define the magnitudes of the direct (V -dependent) and evolving (θ -dependent) effects, respectively. The velocity-dependent term is known to depend on activation energy (Arrhenius relationship) (Rice et al., 2001), and the state (θ)-dependent term is interpreted in terms of changes in real area of contact that scale proportionally to the logarithm of contact age (Ben-david et al., 2010; Dieterich & Kilgore, 1994; Ikari, Carpenter, & Marone, 2016; Perfettini & Molinari, 2017; Svetlizky et al., 2017).

The evolution of friction following a perturbation in slip velocity, for example, during cyclic stick-slip sliding, is defined by the evolution of the state variable θ . When the initial reference state θ_i evolves to $\theta_i + \Delta\theta$, the change in friction $\Delta\mu$ due to the evolving effect only (assuming constant hypothetical slip speed V) is given by

$$\Delta\mu = b \ln\left(\frac{\theta_i + \Delta\theta}{\theta_i}\right) \quad (2)$$

defining a fundamental relation for the rate of frictional healing. Here the evolution of the state, $\Delta\theta$, is defined by the evolution law as discussed below. Equation (2) shows that the magnitude of healing is innately dependent on the initial state θ_i . When an increment of the state $\Delta\theta$ is small compared to the initial state θ_i , equation (2) shows that $\Delta\mu$ approaches zero and the magnitude of frictional healing is negligible.

Laboratory experiments and widely used friction state evolution laws show that friction and frictional state (with dimensions of time) evolve with slip and waiting time during slide-hold-slide motion, yielding a log linear relation between the increase of friction and wait time (Dieterich, 1972; Scholz, 1998). The log linear nature of healing shows that the rate of frictional strengthening is large on weakly healed surfaces (where

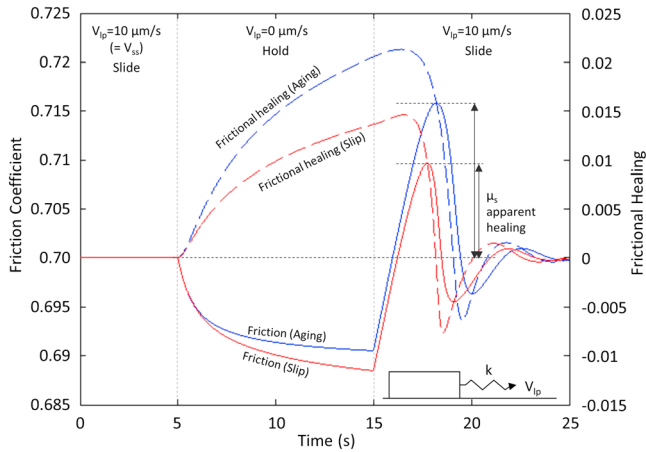


Figure 1. Evolution of friction (solid line) and theoretical frictional healing (dashed line) during a slide-hold-slide experiment for a spring-slider system. Laboratory experiments measure apparent healing, which includes both increased frictional state due to healing during quasi-stationary contact and weakening associated with renewed slip. The red lines are Ruina slip law; the blues lines are Dieterich aging law.

the real area of contact at asperities is small) and conversely small on strongly healed surfaces (e.g., Ikari, Carpenter, & Marone, 2016). For sufficiently short waiting times between slip events, the increase in friction is negligible, which defines a short-term cutoff for frictional healing. This cutoff time is a natural consequence of the logarithmic evolution of frictional state from its initial value. In particular, note that in equation (2), when initial frictional healing is weak (small θ_i), even a small increase in the frictional “state” ($\Delta\theta$) may yield significant healing. Conversely, if the initial frictional healing is strong, a significant evolution of the state ($\Delta\theta$) is required to yield an observable change in friction, implying that the cutoff time should be scaled to the initial state θ_i . Note that this scaling relation may be generally applied to any state evolution law where $\Delta\theta$ evolves with time.

The evolution of the state variable $\Delta\theta$ is described by two widely used laws, denoted (Marone, 1998a), as the Dieterich (aging) law (Dieterich, 1979),

$$\frac{d\theta}{dt} = 1 - \frac{V\theta}{D_c} \quad (3)$$

and the Ruina (slip) law (Ruina, 1983)

$$\frac{d\theta}{dt} = -\frac{V\theta}{D_c} \ln\left(\frac{V\theta}{D_c}\right). \quad (4)$$

Both evolution laws return a positive rate of frictional healing ($d\theta/dt > 0$) for a decrease in slip velocity from steady state ($V < D_c/\theta$). For small perturbations around steady state ($\theta \sim D_c/V$) the two evolution laws are similar but they diverge substantially as velocity approaches zero ($V \ll \theta/D_c$). For the slip evolution law (Ruina), the state variable evolves only at nonzero velocity, while the aging law (Dieterich) delivers maximum healing for a static system ($V = 0$).

Figure 1 shows a quasi-static simulation of slide-hold-slide motion to illustrate the evolution of friction and frictional healing for both state evolution laws. These are conducted with rate and state parameters best fit to the data in Figure 3 (Marone, 1998b) ($\mu_0 = 0.7$, $V_0 = 10 \mu\text{m/s}$, $a = 0.0066$, $b = 0.0083$, and $D_c = 7.1 \mu\text{m/s}$ and with a system stiffness of $k = 1 \times 10^{-3}/\mu\text{m}$ (k is spring stiffness normalized by normal stress)). The system is initially at steady state (for 5 s) with a loading velocity of $V_p = 10 \mu\text{m/s}$ before V_p is decremented to zero for 10 s before the loading again resumes (Figure 1). The solid line denotes the frictional response (rate and state friction; equation (1)), and the dashed line denotes the expected evolution of friction due to healing (equation (2)) from an initial steady state $\theta_i = D_c/V_{ss}$ where V_{ss} denotes steady state velocity prior to hold (i.e., V_p at “slide”). During the hold period, frictional surfaces heal and frictional state θ increases according to the evolution laws (Figure 1), while the measured coefficient of friction decreases because the direct frictional effect (associated with the decrease in slip velocity) dominates over the state evolution healing effect. When loading resumes, the velocity effect and the state evolution that occurred during the hold period are immediately apparent (Figure 1) and together yield a peak value of friction, which in past studies was referred to as time-dependent static friction (e.g., Coulomb, 1785; Rabinowicz, 1951, 1956).

In the laboratory and on tectonic faults, the effect of frictional healing on shear strength is defined by the observed peak strength. In laboratory slide-hold-slide (SHS) experiments, $\Delta\mu$ (“apparent” healing) is defined as the difference between peak friction and the initial steady state friction (Figure 1). Figure 1 shows that peak friction in a SHS test is determined by both “actual” frictional healing (dashed line) and the reduction in frictional strength associated with the decrease in frictional state during the acceleration stage before the peak.

Laboratory observations of apparent healing have a linear relation with the logarithm of hold time t_h and may be represented by two constants t_c and β (Dieterich, 1972),

$$\mu_s = \beta \ln\left(\frac{t_h}{t_c} + 1\right) \quad (5)$$

where t_c denotes cutoff time and β denotes the log linear healing rate. Note that equation (5) is typically expressed with \log_{10} , but we use natural log for consistency with rate and state healing and so that

equations (2) and (5) are described in the same form. Slide-hold-slide experiments confirm that t_c is dependent on steady state slip velocity (V_{ss}) prior to hold (Marone, 1998b). Also, t_c may be dependent on a characteristic length scale for the asperity population, often defined as “ D_c ,” which is strongly connected to D_c (Marone et al., 2009; Nakatani & Scholz, 2006). Both of these (V_{ss} and D_c) dependencies are implied from rate and state healing. In typical slide-hold-slide experiments, the system is set to steady state prior to the application of a hold, i.e., $\theta_i = D_c/V_{ss}$, and equation (2) indicates that the magnitude of healing is intrinsically dependent on θ_i .

Comparing the change in frictional state $\Delta\theta$ with laboratory healing observation would allow the constants t_c and β to be defined and may suggest which evolution law returns better results. Intriguingly, both evolution laws provide plausible results corresponding to the laboratory observations. The Dieterich aging law innately represents log linear frictional strengthening for stationary contact. Equation (3) describes $d\theta \sim dt$ when sliding velocity decreases rapidly from an initial condition of steady state sliding. Substituting this relation into equation (2) shows, quite simply, that log linear healing occurs when dt is larger than the initial frictional state θ_i . Conversely, for the Ruina slip law, healing only evolves at finite velocity, such as would be expected during quasi-static creep. Although the “hold” period in an SHS experiment begins when loading rate is set to zero, the slider velocity never actually reaches zero for a system with finite stiffness. Instead, the fault slip rate and the shear force driving slip decrease continuously with creep motion. Numerical studies indicate that both state evolution laws can plausibly explain laboratory observed healing with time (Bhattacharya, Rubin, & Beeler, 2017; Marone & Saffer, 2015).

The desired evolution law may be determined by other (non-SHS) experimental observations. However, existing evidence is still ambiguous. The response to the Dieterich aging law is supported by direct observation, where the contact area between two stationary surfaces increases in accordance with the description of the aging law (Dieterich & Kilgore, 1994). Conversely, recent observations from friction response with large velocity steps favor the use of the slip law (Bayart, Rubin, & Marone, 2006; Bhattacharya et al., 2015; Rathbun & Marone, 2013).

For either law, the complete description of frictional strength recovery with time and (creep) slip, given by equation (5), depends on the full suite of rate and state parameters a , b , D_c , and the elastic stiffness of the fault zone and surroundings (see Marone & Saffer, 2015, for a recent review). Although critical evaluation of the state evolution law, with possible modification, is beyond the scope of this study, we focus on the need to better understand the origin of log linear healing and the term t_c of equation (5). Here we employ numerical experiments and RSF laws to study frictional healing, with particular focus on the parameter t_c . We show that t_c can be predicted by the initial value of frictional state θ_i in equation (2) for both of the state evolution laws.

Rate and state friction laws indicate that fault healing is observed when $\Delta\theta$ is comparably larger than the initial frictional state θ_i (i.e., D_c/V_{ss} during slide-hold-slide experiments where V_{ss} denotes V_p prior to hold). We conducted simulations to illustrate the dependency of healing on the parameters D_c and V_{ss} (Figure 2). These numerical investigations simulate apparent frictional healing during SHS tests for a range of D_c and sliding velocity values. Figure 2 shows the behavior for both state evolution laws and RSF parameters $a = 0.007$, $b = 0.01$, and $k = 3 \times 10^{-3}/\mu\text{m}$ (where k is the elastic stiffness normalized by stress). Figure 2a shows the evolution of healing as a function of D_c (1, 100 μm), and Figure 2b shows the behavior as a function of V_{ss} (1 and 10 $\mu\text{m/s}$).

Healing rates (slopes) predicted from the two evolution laws are substantially different (Figure 2). With the Dieterich aging law, healing rate (per decade) approaches to an asymptote $b\ln(10)$ (i.e., $\mu_s \sim b\ln(t_h)$) at long holds, corresponding to previous studies (e.g., Beeler et al., 1994; Marone & Saffer, 2015) and recent arguments by Bhattacharya et al. (2017). The healing rate is smaller for the Ruina slip law and is significantly dependent on D_c (Figure 2a). Also, the healing rate slightly increases with duration of hold time for the slip law (especially with large D_c). Although the slip law appears to violate the log linear nature of healing, we note that the non-linearity is greatest at early times, which is consistent with laboratory observations, and such healing rate increases at long hold times are also experimentally reported (e.g., Carpenter et al., 2014; Ikari, Carpenter, Vogt, et al., 2016).

Notably, the healing rate simulations can be rescaled to reveal a nondimensional hold time or hold-slip, consistent with previous work (Marone, 1998b; Marone & Saffer, 2015). Figure 2 shows that the SHS healing data

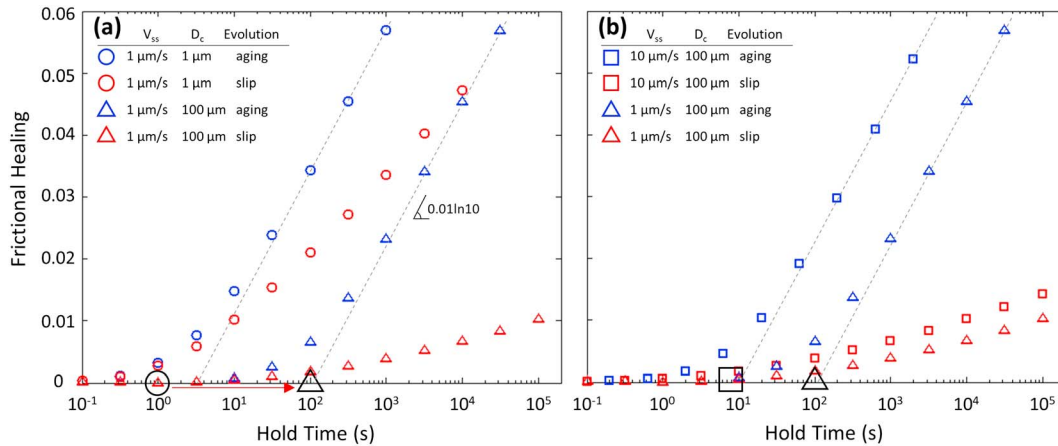


Figure 2. Numerical simulation results of apparent healing in SHS experiments. $K/\sigma = 3 \times 10^{-3}/\mu\text{m}$ (normalized stiffness) $a = 0.007$, and $b = 0.01$ with (a) 2 orders-of-magnitude change in D_c and (b) 1 order-of-magnitude change in V_{ss} . The symbol colors and shapes denote different input parameters (see key). The black symbols on x axis represent D_c/V_{ss} values of each corresponding case. The dashed lines on aging law are back-projected healing rates based on the two longest hold times in each case.

translate horizontally in proportion to the initial state θ_i regardless of the evolution law. The symbols of Figure 2 represent different combinations of V_{ss} and D_c as, circles: $V_{ss} = 1 \mu\text{m/s}$ and $D_c = 1 \mu\text{m}$, triangles: $V_{ss} = 1 \mu\text{m/s}$ and $D_c = 100 \mu\text{m}$, and squares: $V_{ss} = 10 \mu\text{m/s}$ and $D_c = 100 \mu\text{m}$. The larger, black symbols on the x axis represent D_c/V_{ss} values for each case (Figure 2). The linear trend lines on the aging law (dashed lines), which correspond to long-term asymptotic healing rates of previous studies (Bhattacharya et al., 2017), present cutoff times that scale with the ratio D_c/V_{ss} . A 2 order of magnitude increase in D_c yields a 2 order increase in the cutoff time (Figure 2a), and a 1 order of magnitude decrease in velocity yields a 10 times increase of cutoff time (Figure 2b). Although the trend line cannot be defined from slip law healing, due to its nonlinear nature, it is clearly shown that the curves translate horizontally depending on the initial value of frictional state θ_i .

According to this scaling relation for the cutoff time, assuming log linear healing, an approximate rate and state frictional healing law may be represented as

$$\mu_s = \beta \ln \left(1 + \frac{t_h}{\alpha D_c/V_{ss}} \right) \quad (6)$$

where α is a parameter that describes the offset between the cutoff time and D_c/V_{ss} (that is, between the x intercepts of trend lines and their D_c/V_{ss} on the x axis in Figure 2). In a strict sense, equation (6) is only valid for the aging law, due to the nonlinear nature of the slip law. But we note that slip law healing with small D_c can be (miss-) interpreted as asymptotic on a log linear plot. The offset α in equation (6) is dictated by the response time of a system with finite stiffness and, if the system is governed by the slip law, the intrinsically slow rate of state evolution for the slip law may further increase α (moves the curves to the right). In these simulations with the aging law, α is no more than an order of magnitude from unity.

This view assumes that the frictional system obeys RSF with constant parameters. Although this assumption may be acceptable in typical slide-hold-slide experiments, it may not always be valid in nature. Delay or promotion of healing has been observed under hydrothermal condition (Chen & Spiers, 2016; Giger, Cox, & Tenthorey, 2008; Karner, Marone, & Evans, 1997; Nakatani & Scholz, 2004; Tenthorey & Cox, 2006) and also as a result of the activation of pressure solution (Niemeijer, Marone, & Elsworth, 2008; Yasuhara et al., 2005).

Figure 3 compares laboratory-observed healing in SHS experiments (Marone, 1998b) with the modified healing law of equation (6) for two sliding velocities ($V_{ss} = 1$ and $10 \mu\text{m/s}$). Separately conducted velocity stepping experiments (upper left box) show a critical distance $D_c \sim 7.1 \mu\text{m}$. Substituting V_{ss} and D_c with the fitting parameters $\beta = 0.0042$ and $\alpha = 1$ into equation (6) yields the solid lines of Figure 3, which match the laboratory observations (circles) reasonably well.

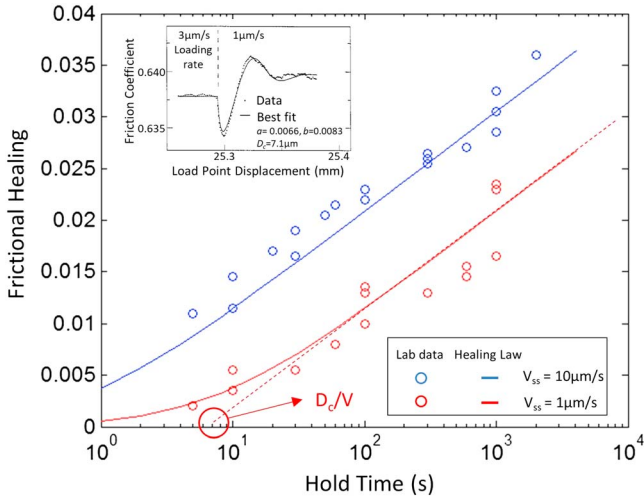


Figure 3. Comparison of laboratory measurements of apparent frictional healing (Marone, 1998b) and equation (6). The blue and red symbols represent different loading velocities of $V_{ss} = 10 \mu\text{m/s}$ and $V_{ss} = 1 \mu\text{m/s}$, respectively. For the healing law, $D_c \sim 7.1 \mu\text{m}$ as measured from velocity stepping experiments (upper left box) in the same study. The solid lines are calculated from equation (6) using $D_c = 7.1 \mu\text{m}$, $\beta = 0.0042$, and $\alpha = 1$. The dashed line is the back-projected trend based on the longest hold times. The plot indicates that D_c/V_{ss} provides a good approximation for the short time cutoff of frictional healing.

3. Numerical Method of Stick-Slip Simulation

In the foregoing we have shown that frictional healing is strongly dependent on the critical slip distance D_c and antecedent slip velocity. This implies that the higher the slip velocity of a preceding earthquake, the larger the immediate frictional healing. Accordingly, in the case of large values of dynamic slip velocity, one would expect a longer interseismic duration and a longer stick-slip recurrence interval—this in turn would result in greater frictional healing and produce a larger stress drop for the anticipated failure (earthquake) event. In the following, we analyze laboratory earthquakes (stick-slip motion) using a unique numerical solution of spring-slider RSF behavior that also accommodates inertia. Uniquely, this solution spans the full inertial spectrum from slow to fast slip (see Figures S1 and S2 in the supporting information), allowing the exploration of relations between healing, recurrence time, and stress drop.

In a one dimensional spring-slider system (Figure 4), the Newtonian force balance governing motion is

$$M\ddot{\delta} = K(\delta_{lp} - \delta) - \mu\sigma \quad (7)$$

where δ is displacement of the slider, δ_{lp} is displacement of the load point, M is mass per unit area (kg/m^2), K is spring stiffness (Pa/m), and σ is normal stress.

Although the stick-slip motion can be simply defined by coupling three equations (force balance (equation (7)), rate and state (equation (1)), and an evolution law (equations (3) or (4)), full solutions for an inertia-dominated system are difficult due to the numerical instability present in the dynamic acceleration process. To condition and thereby improve this stability, we made use of a constant friction solution (e.g., Johnson & Scholz, 1976). With constant friction μ and load point displacement δ_{lp} and for initial displacement δ_{ini} and velocity V_{ini} , the solution of equation (7) results in a harmonic oscillation as

$$\delta(t) = (\delta_{ini} - F) \cos(\omega t) + \frac{V_{ini}}{\omega} \sin(\omega t) + F \quad (8)$$

where ω is angular velocity defined as $\omega = \sqrt{K/M}$ and $F = \delta_{lp} - \mu\sigma/K$.

We may discretize this equation in time Δt by updating displacement and velocity in each time step as

$$\delta^{i+1} = [\delta^i - (\delta_{lp}^{i+1} - \mu^{i+1}\sigma/K)] \cos(\omega\Delta t) + \frac{V^i}{\omega} \sin(\omega\Delta t) + (\delta_{lp}^{i+1} - \mu^{i+1}\sigma/K) \quad (9)$$

where superscripts i and $i + 1$ denote time steps. Note that load point displacement δ_{lp} can be time-dependent in this form since force in the spring is recalculated in every time step (δ^i is updated). Here friction μ is also discretized in time for further coupling with the rate and state law.

Equation (9) directly provides the displacement in the following time step δ^{i+1} , which can be resubstituted for time step $i + 2$. To acquire V^{i+1} , we use the midpoint velocity $V^{i+1/2}$ and acceleration as

$$V^{i+1/2} = \frac{\delta^{i+1} - \delta^i}{\Delta t} \quad (10)$$

Acceleration between time steps i and $i + 1/2$ is

$$a = \frac{V^{i+1/2} - V^i}{\Delta t/2} \quad (11)$$

Assuming that this acceleration is extended to time step $i + 1$, the velocity at $i + 1$ is

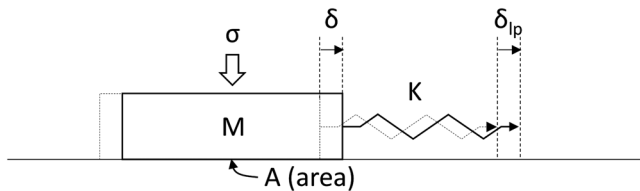


Figure 4. Spring-slider system, where δ is displacement of the slider, δ_{lp} is displacement of a load point that drives slip, M is mass per unit area, K is spring stiffness, and σ is normal stress and A is frictional (contact) surface area. Note that the gravitational force is associated with normal stress but accommodated separately in the inertial term.

$$V^{i+1} = V^i + a\Delta t = 2 \frac{(\delta^{j+1} - \delta^j)}{\Delta t} - V^i. \quad (12)$$

We confirm that coupling in equations (9) and (12) provides an equivalent solution to equation (8) for small time steps Δt , and therefore solves the force balance of equation (7). Now we further couple the calculated displacement and velocity with rate and state friction. To accomplish this, we begin each time step with the state evolution law. For the Dieterich aging law, we have

$$\theta^{j+1} = \theta^j + \left(1 - \frac{V^{i+1}\theta^j}{D_c}\right)\Delta t \quad (13)$$

and for the Ruina slip law we have

$$\theta^{j+1} = \theta^j - \left[\frac{V^{i+1}\theta^j}{D_c} \log\left(\frac{V^{i+1}\theta^j}{D_c}\right)\right]\Delta t. \quad (14)$$

For numerical simplicity, we use time step i to update the state variable (i.e., $V^{i+1} \cdot \theta^j$ in equations (13) and (14)), but a preferred choice will be $V^{i+1} \cdot \theta^{j+1}$ to make the procedure fully implicit. With the Dieterich aging law, the expression for θ^{j+1} can be simply acquired by substituting $V^{i+1} \cdot \theta^{j+1}$ and rearranging equation (13). An additional numerical procedure is required with the Ruina slip law.

Rate and state friction can be discretized as

$$\mu^{i+1} = \mu_0 + a \ln\left(\frac{V^{i+1}}{V_0}\right) + b \ln\left(\frac{V_0\theta^{j+1}}{D_c}\right) \quad (15)$$

To track friction as a function of slip and time, we couple equations (13) or (14), (15), (9), and (12) and solve them simultaneously using the Newton-Raphson method until the velocity V^{i+1} converges. We find that the solution satisfies force balance, as illustrated in the following example.

In this method, the velocities in each numerical step are constrained within the solution imposed by force balance ($\Sigma F = ma$). This increases convergence rate and numerical stability. Although restricted here to the two widely used evolution laws with constant frictional parameters, the method could be extended to accommodate other evolution laws (e.g., Linker & Dieterich, 1992; Nagata et al., 2012)—and also accommodate strain, slip rate, and temperature dependencies of frictional parameters (e.g., Ikari, Marone, & Saffer, 2011; Niemeijer et al., 2016; Svetlizky et al., 2017).

4. Simulation Results

We conduct a series of numerical simulations using the approach outlined above to illuminate the dependency of healing on prescribed rate and state parameters a , b , D_c , and loading rate V_{lp} . To generate unstable stick-slip motion, we set $a - b < 0$ and $K < K_c$. Here K_c is a critical stiffness that determines slip stability. The critical stiffness of spring slider moving in steady state at velocity V is defined as (Gu et al., 1984; Rice & Ruina, 1983; Roy & Marone, 1996)

$$K_c = \frac{(b-a)\sigma}{D_c} \left[1 + \frac{MV^2}{\sigma a D_c}\right] \quad (16)$$

The “dynamic” term (second term in brackets in equation (16)) is negligible in the following study, but we note that it indeed influences stability of stick-slip system (see Figure S2).

In all simulations, initial velocity and frictional state are set to $V_{ini} = V_0$ and $\theta_{ini} = D_c/V_0$, and consequently, initial friction is μ_0 (see equation (1)). Given that the arbitrary reference velocity is set as $V_0 = 10^{-9}$ m/s, the initial frictional state ($\theta_{ini} = D_c/V_0$) is much larger than at steady state for typical laboratory loading rates $V_{lp} = 10\text{--}1,000$ $\mu\text{m/s}$. Thus, this represents strongly healed surfaces. All simulations initially demonstrate large stress drop due to this strong healing, but the stress drop decreases with the sequence of stick-slip motion and becomes periodic (Figure 5). Simulation results with the same set of input parameters yield identical periodic motions regardless of the initial parameter values.

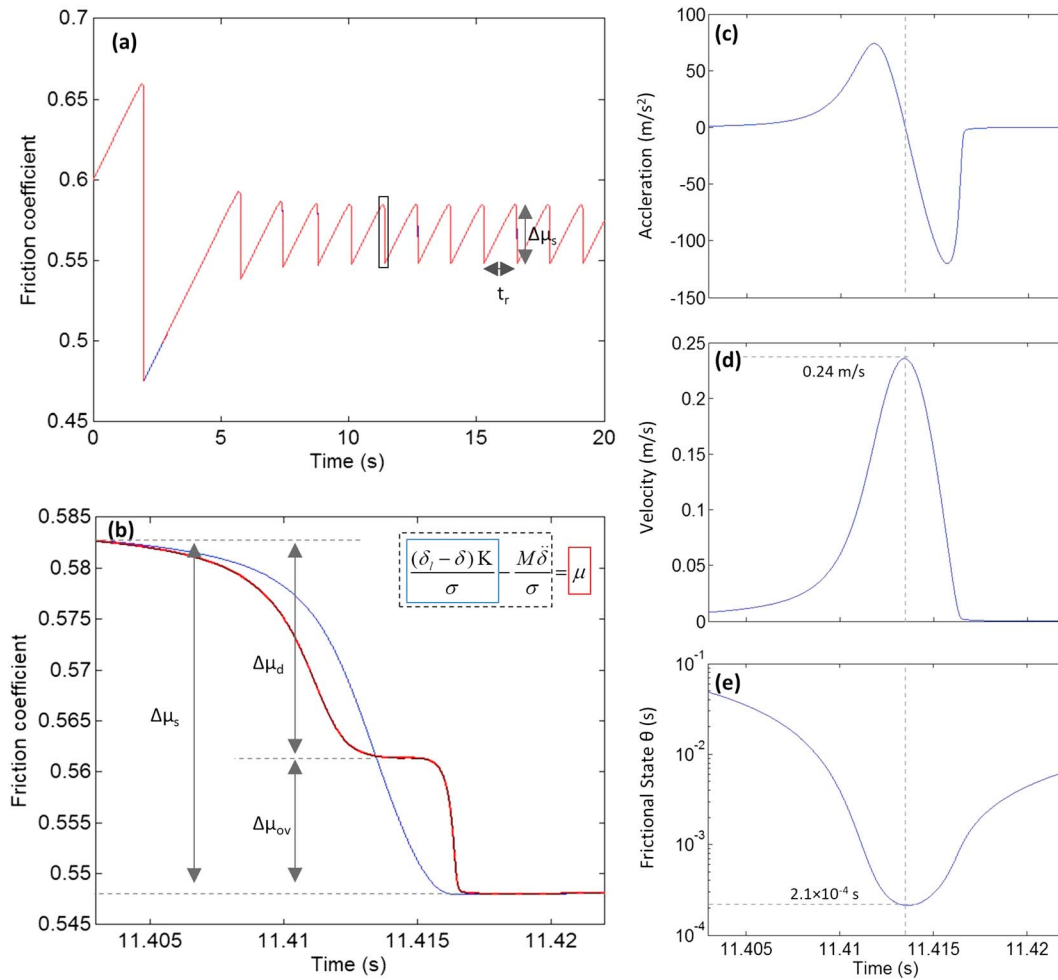


Figure 5. Simulation result of stick-slip motion. (a) Repeated stress buildup and friction-drop during a 20 s period from the initial state. (b) Enlargement of one friction drop (rectangle in Figure 5a). The red, blue, and black lines denote corresponding terms in the force balance equation shown in the upper inset. Note that red and black curves overlap. The blue curve represents normalized shear stress. (c–e) Velocity, acceleration, and state variable during the same period highlighted in Figure 5b. Note that state is minimum when slip velocity is maximum and that acceleration/deceleration history is asymmetric.

4.1. Stick-Slip Behavior

Figure 5 show results of stick slip with input parameters $\mu_0 = 0.6$, $a = 0.005$, $b = 0.007$, $D_c = 50 \mu\text{m}$, $\theta_{\text{initial}} = 50,000 \text{ s}$, $\sigma = 1 \text{ MPa}$, $K = 32 \text{ MPa/m}$ ($0.8K_c$), $V_p = 1 \text{ mm/s}$, and $M = 100 \text{ kg/m}^2$ for the aging law. Figure 5a illustrates stick-slip frictional behavior for 20 s. The magnitude of the initial frictional drop is significant, due to its high initial healing. The stick-slip behavior becomes nearly perfectly periodic after several cycles. Figures 5b–5e show enlargements of the stick-slip event that is boxed in Figure 5a. Each curve in Figure 5b denotes a segment of the normalized force balance equation

$$\frac{(\delta_l - \delta)K}{\sigma} - \frac{M\ddot{\delta}}{\sigma} = \mu \quad (17)$$

which is identical to the Newtonian force balance (equation (7)). The blue curve (Figure 5b) denotes the apparent friction (or normalized shear stress, which is the first term on the left-hand side of equation (17)), and the red curve (note that it overlaps the black dashed curve) denotes the actual (rate and state) friction, which is the right-hand side of equation (17). Because the two frictional magnitudes differ due to the large (normalized) inertial force (the second term of the left-hand side of equation (17)), significant decoupling occurs in dynamic slip, with offset proportional to acceleration (Figure 5c). The entire left-hand side of equation (17) is calculated with acceleration (Figure 5c) and plotted with the black dashed curve. The curve completely overlaps the red curve in Figure 5b, confirming that force balance (equation (17)) is satisfied.

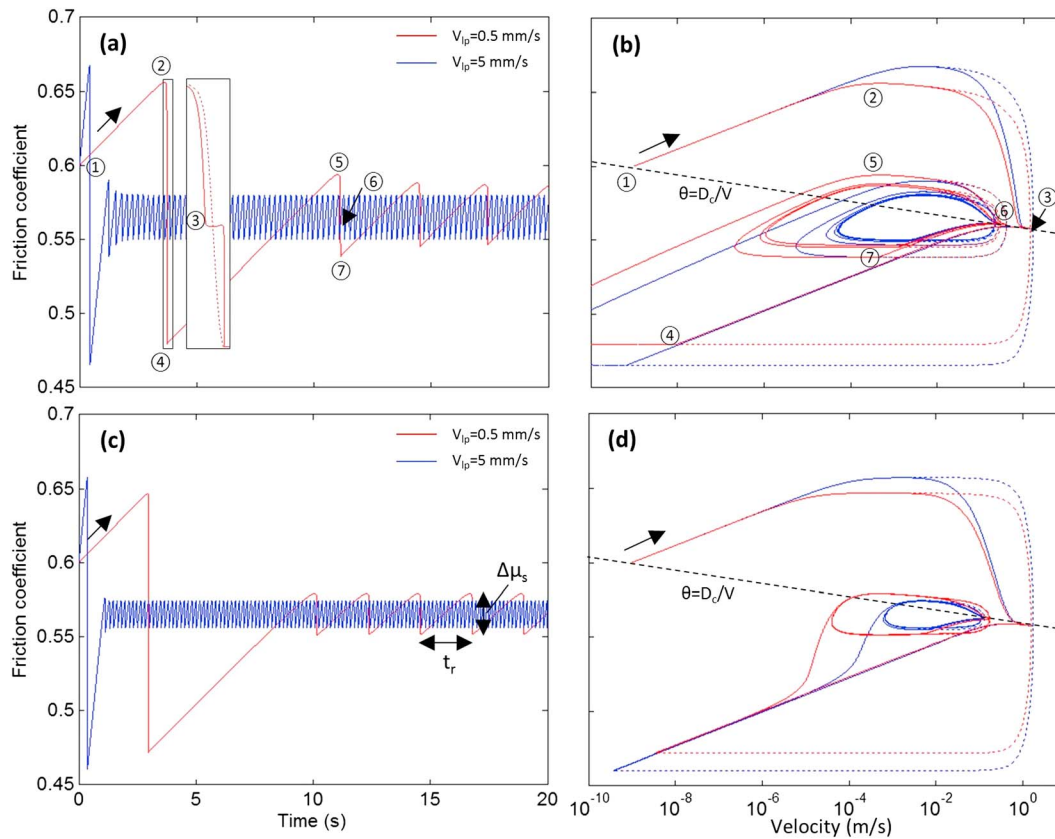


Figure 6. Friction response and corresponding phase plane plot (friction-velocity) during stick-slip motion with (a and b) the aging law and (c and d) the slip law. The red lines show loading velocity of 0.5 mm/s, and the blue lines show loading velocity of 5 mm/s. In each case the simulation started from an initial condition of steady sliding at $V = 10^{-9}$ m/s. Inset in Figure 6a shows a zoom-in of the first stick-slip event for loading at 0.5 mm/s. The numbers in upper panels provide fiducial points for comparison. Note that a steady state stick-slip limit cycle is reached in each case and that the friction drop and velocity excursions scale inversely with loading velocity, reflecting greater frictional healing for lower loading rate.

The process of inertia-controlled friction drop can be divided into acceleration and deceleration stages (Gu et al., 1984; Gu & Wong, 1991). The acceleration is driven by a decrease in frictional state (Figure 5e) in response to increasing velocity. Due to the rapid drop in the frictional state term, the frictional resistance (Figure 5b red) becomes smaller than the normalized shear stress (Figure 5b blue) and consequently the system accelerates. The magnitude of the friction drop in this acceleration stage is defined as the dynamic friction drop, $\Delta\mu_d$ (see Figure 5b). Frictional healing (θ increase) begins at the conclusion of this dynamic friction drop (Figure 5e). However, normalized shear stress (apparent friction) continues to decrease due to the inertial effect (e.g., Beeler et al., 2001). Actual RSF sharply decreases at the conclusion of the slip process due to the velocity effect. This latter part of the friction drop is defined as dynamic overshoot $\Delta\mu_{ov}$, and the total friction drop is defined as the static friction drop, $\Delta\mu_s (= \Delta\mu_d + \Delta\mu_{ov})$; see Figure 5b).

Healing begins at the conclusion of the dynamic friction drop; thus, the minimum (and therefore initial) value of frictional state can be observed at maximum velocity. In this specific simulation, the observed minimum value of frictional state is $\theta_i \sim 2.1 \times 10^{-4}$ s (Figure 5e) with a peak velocity of $V_{peak} \sim 0.24$ m/s (Figure 5d). Using an input parameter of $D_c = 5 \times 10^{-5}$ m, we find that the steady state relationship $\theta = D_c/V_{peak}$ is satisfied at the initiation of frictional healing.

4.2. Evolution Laws and Phase Diagram

We show simulation results for each state evolution law and for two loading velocities ($V_{ip} = 0.5$ and 5 mm/s) in Figure 6. The other RSF parameters are identical to the previous simulation (Figure 5). Figures 6a and 6c represent full stick-slip friction behavior, and Figures 6b and 6d represent phase diagrams (friction-velocity) of actual friction (rate and state friction, solid line) and apparent friction (normalized shear stress, dashed line). The black dashed lines in the phase diagrams represent steady state where the relation $\theta = D_c/V$ is satisfied.

Point ① in Figures 6a and 6b represents the initial state, which represents input values $V_{ini} = V_0$ (10^{-9} m/s), $\theta_{ini} = D_c/V_0$ and accordingly, from the rate and state law (equation (1)) $\mu = \mu_0$ (0.6). Friction builds until the slider velocity reaches the loading velocity ① → ② (for the case with $V_p = 0.5$ mm/s). During the dynamic friction drop, velocity rapidly increases, and accordingly, both actual friction (solid line) and apparent friction (dashed line) decouple due to a large inertial force ② → ③ (highlighted in box in Figure 6a). At this point, friction temporarily reaches a steady state (Figure 6b, black dashed line) at maximum velocity ③ and dynamic overshoot follows ③ → ④. This frictional buildup and drop is repeated, but this time, with a reduced size of the loop in the phase diagram (④ → ⑤ → ⑥ → ⑦). Note that the magnitude of the friction drop decreases in successive sequences and ultimately stabilizes to a periodic behavior (Figure 6).

These simulations demonstrate that greater healing yields longer recurrence time and larger stress drop. For an initially elevated frictional state ($\theta = 50,000$ s) we find a large initial friction drop in all simulations. Also, the magnitude of the friction drop during periodic motion is larger for slower loading (Figure 6), reflecting that a higher degree of healing is induced by a longer recurrence time. Similarly, stress drop and recurrence time are larger and longer with the aging law (Figure 6a) compared to the slip law (Figure 6c) due to the higher healing rate (see Figures 1 and 2).

In all simulations, the frictional system remains temporarily at steady state (black dashed line in Figures 6b and 6d) at the peak velocity of each slip. Accordingly, we can utilize the relationship $\theta_i = D_c/V_{peak}$ to calculate the minimum value of the state variable for each event. Previously, we have shown that frictional healing is strongly dependent on the initial value of the frictional state, and therefore, it is expected that the evolution of stress drop during stick-slip motion may also scale to this initial (minimum) value of state $\theta_i (=D_c/V_{peak})$.

4.3. Recurrence and Friction Drop

Figure 6 shows that a greater friction drop ($\Delta\mu_s$) is associated with a longer recurrence time (t_r). This is consistent with laboratory data on stick-slip motion, where static stress drop $\Delta\mu_s$ shows a logarithmic dependence on event recurrence time t_r in periodic motion (e.g., Beeler et al., 2001, 2014; Ben-david et al., 2010; Karner & Marone, 2000)

$$\Delta\mu_s = (b - a)(1 + \zeta) \ln \frac{t_r}{t_0} \quad (18)$$

where t_0 is the empirical cutoff recurrence interval at a projected zero stress drop and ζ represents a factor primarily related to the influence of dynamic overshoot. Equation (18) shows that the slope of the slip-magnitude relation scales with the RSF parameter $(b - a)$ with a factor of $(1 + \zeta)$. The common log linear dependency of stick-slip (equation (18)) and healing (equations (5) or (6)) suggests that the cutoff recurrence interval to a back projected zero stress drop (t_0) may also be scaled with the frictional state at the beginning of healing; this is given by the numerical simulation that $\theta_i = D_c/V_{peak}$.

We conducted multiple stick-slip simulations to determine the relationship between cutoff time and the parameter D_c/V_{peak} . A normal stress $\sigma = 2$ MPa was applied for all cases in Figures 7a–7d except $\sigma = 20$ MPa for $D_c = 500$ μm to prevent the critical stiffness K_c from becoming too small (equation (16)). The recurrence time is conditioned by loading velocity—this is varied from 10 $\mu\text{m/s}$ to 1 mm/s (Figure 7a), except for the case of $D_c = 500$ μm where it is varied from 1 mm/s to 2 cm/s (Figure 7c). The red and blue symbols and trend lines represent the slip and aging laws, respectively.

We document the evolution of static friction drop versus recurrence time (equation (18)) for a series of repetitive stick-slip events (Figure 7). Results reported in each panel (Figure 7) use the same parameters except that we vary the RSF parameters a and b (Figures 7a and 7b), critical distance D_c (Figures 7c and 7d), and critical spring stiffness (Figures 7e and 7f). In Figures 7e and 7f, we vary the critical stiffness to explore a range of peak slip velocities during failure, since the stick-slip velocity can be controlled by the ratio of system stiffness and critical stiffness K/K_c (e.g., Leeman et al., 2016). To mimic the procedure used in laboratory experiments, we use a constant spring stiffness ($K = 640$ MPa/m) and vary normal stress to change the critical stiffness over the range of $\sigma = 2$ MPa, 1.68 MPa, and 1.61 MPa yielding $K = 0.8K_c$, $K = 0.95K_c$, and $K = 0.99K_c$, respectively. All plots clearly show that the magnitude of friction drop increases linearly with the logarithm of recurrence time.

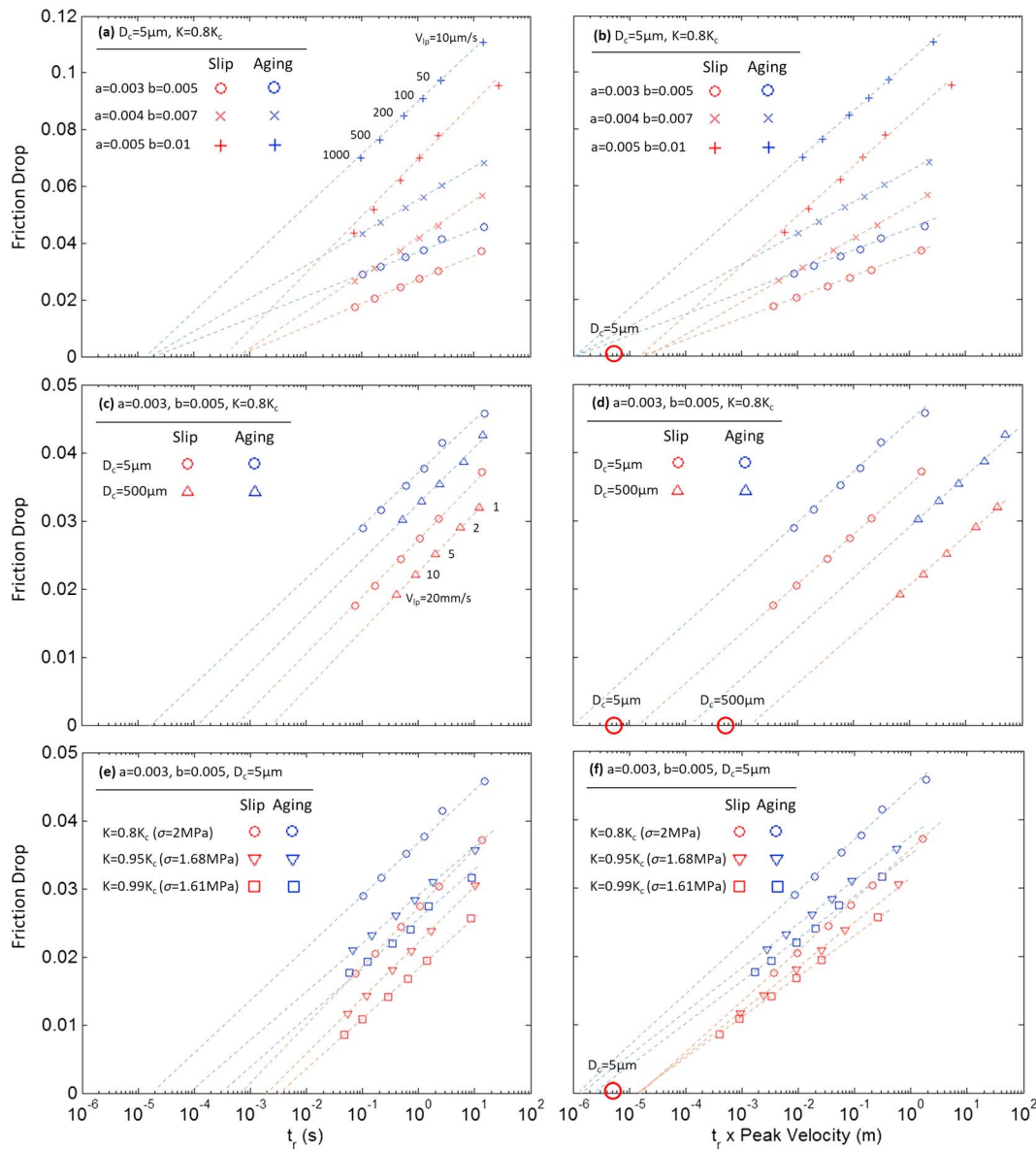


Figure 7. Results of stick-slip simulations (e.g., Figure 6). (Static) Friction drop $\Delta\mu_s$ in periodic motion is plotted versus recurrence time (left-hand set of panels) and versus product of recurrence time and peak slip velocity (right-hand panels). Three sets of parameters are studied: (a and b) RSF parameters a and b , (c and d) critical distance D_c , and (e and f) stiffness. The red denotes the slip law, and the blue denotes the aging law. Recurrence time is varied via loading rate which ranges from 10 to 1,000 $\mu\text{m/s}$ in all cases except the case for $D_c = 500 \mu\text{m}$ (triangle) in Figures 7c and 7d. Loading rates are marked in Figures 7a and 7c. The red circles in Figures 7b, 7d, and 7f show that the short-term cutoff for interevent frictional healing clearly scales with D_c .

Table 1 provides our parameter values and the results for the evolution of static stress drop in periodic motion. The evolution rates (stated in natural log $\ln(t_r)$ to enable direct comparison with equation (18)) and cutoff values for each set of simulations are also given in Table 1. Note that the log linear evolution rates of friction drop are not distinct between aging and slip law cases, which is in contrast to observations of slide-hold-slide healing (Figure 2). This was similarly reported in previous numerical simulation results (Beeler et al., 2001; He et al., 2003) and shows that the state evolution for healing based on SHS and stick slip seems to follow a somewhat different path. The healing rates are close to $2(a - b)$ with both evolution laws, which yields $\zeta \sim 1$ in equation (18). Note that ζ embodies more than just dynamic overshoot. The simulation results show that the ratio of dynamic to static stress drop (expressed as friction drop $\Delta\mu_d/\Delta\mu_s$) varies in the range of 0.6–0.75, indicating that the dynamic friction drop is larger than the frictional overshoot in the simulations (see Figure 5b for ratio of $\Delta\mu_s$, $\Delta\mu_d$, and $\Delta\mu_o$).

Table 1
Simulation Input and Resulting Slope of the Natural Logarithm and x Intercept of the Friction Drop Trend Line (Figure 7)

Evolution law	D_c (μm)	a	b	K/K_c	Fric. drop versus t_r (Figures 7a, 7c, and 7e)		Fric. drop versus $t_r \times V_{\text{peak}}$ (Figures 7b, 7d, and 7f)	
					Slope $\ln(t_r)$	Cutoff (s)	Slope $\ln(t_r V)$	Cutoff (m)
Slip law	5	0.003	0.005	0.80	0.0038	7.79×10^{-4}	0.0032	1.52×10^{-5}
	5	0.004	0.007	0.80	0.0058	8.08×10^{-4}	0.0049	2.13×10^{-5}
	5	0.005	0.01	0.80	0.0088	4.31×10^{-4}	0.0077	1.88×10^{-5}
	500	0.003	0.005	0.80	0.0038	2.68×10^{-3}	0.0032	1.76×10^{-3}
	5	0.003	0.005	0.95	0.0036	2.22×10^{-3}	0.0029	1.79×10^{-5}
	5	0.003	0.005	0.99	0.0033	3.79×10^{-3}	0.0026	1.43×10^{-5}
Aging law	5	0.003	0.005	0.80	0.0034	1.93×10^{-5}	0.0032	9.72×10^{-7}
	5	0.004	0.007	0.80	0.0050	1.70×10^{-5}	0.0047	1.05×10^{-6}
	5	0.005	0.01	0.80	0.0081	1.65×10^{-5}	0.0076	1.22×10^{-6}
	500	0.003	0.005	0.80	0.0037	1.62×10^{-4}	0.0032	1.52×10^{-5}
	5	0.003	0.005	0.95	0.0030	6.55×10^{-5}	0.0028	1.58×10^{-6}
	5	0.003	0.005	0.99	0.0029	1.57×10^{-4}	0.0032	1.52×10^{-5}

The simulation results suggest that the cutoff time during stick-slip evolution is indeed dependent on D_c and V_{peak} . With the same evolution law, the observed cutoff values clearly diverge when D_c and V_{peak} are different (Figures 7c and 7e), while they are roughly identical with similar value of D_c and V_{peak} (Figure 7a). The difference between aging and slip laws can clearly be observed in the cutoff behavior. Using the same input parameters, the aging law always yields an approximately 1 order-of-magnitude smaller cutoff time, yielding larger friction drop at a given recurrence time.

Figures 7b, 7d, and 7f represent the same friction drop with respect to Figures 7a, 7c, and 7e with peak velocity scaling on the recurrence time of each periodic event. This is intended to remove the velocity effect on the cutoff behavior so that the observed cutoff value can be directly scaled to D_c . Assuming that the stick-slip evolution has a cutoff time at D_c/V_{peak} (i.e., $\Delta\mu_s \sim \ln(t_r/(D_c/V_{\text{peak}}))$), then the cutoff value in the plot $\Delta\mu_s$ versus $\ln(t_r \times V_{\text{peak}})$ is required to scale with D_c only. The plots clearly indicate that all cutoff values of the log linear trend line are back projected around their input D_c (red circle) value. In the D_c control group (Figure 7d), the cutoff values of each evolution law are located adjacent to their input D_c values ($D_c = 5 \mu\text{m}$ and $500 \mu\text{m}$). The ranges of cutoff times in Figure 7e converge around D_c after multiplication by V_{peak} (Figure 7f). These results clearly show that the cutoff time in the evolution of friction drop also scales with D_c/V_{peak} similar to the cutoff behavior during the hold portions of slide-hold-slide experiments.

5. Experimental Observations

We perform double direct shear experiments at two different normal stresses of 5 MPa and 7 MPa to confirm the validity of the numerical simulation results. A decrease in normal stress reduces the critical stiffness (equation (16)) and consequently enhances system stability. Laboratory observations on the spectrum of stick-slip modes (Leeman et al., 2016; Scuderi et al., 2016) show that peak slip velocity in the dynamic slip mode drops significantly as system stiffness (K) approaches the critical stiffness (K_c). Using this phenomenon, we successfully generate stick-slip motions with two groups of distinct peak velocities (Figure 8). Stick-slip motions with normal stress of 5 MPa always exhibit slow stick-slip ($V_{\text{peak}} < 100 \mu\text{m/s}$), while at 7 MPa, the behavior evolves from initially slow (but still faster than the 5 MPa case) to regular (V_{peak} on the order of cm/s) stick slip (Figures 8c and 8d). Further details of the experimental method are reported in Leeman et al. (2016). An identical experimental configuration and conditions are used except that the loading velocity is varied in these experiments to control the recurrence time (see V_p in Figures 8a and 8b).

Figure 8e represents evolution of friction drop with recurrence time (crosses: 7 MPa, circles: 5 MPa). The stick-slip motions are not perfectly periodic—rather they are spread vertically—but the magnitude of the stress drop increases with the logarithm of recurrence as observed in the numerical study. This vertical spread is significantly contributed by variation in the peak slip velocity. The friction drop evolution with slow slip (5 MPa) is clearly delayed over that of faster slip (7 MPa). This evolution of slip magnitude clearly represents that when peak velocity is high (i.e., at 7 MPa), friction drop is greater within a given recurrence interval. The behavior resembles laboratory observations of the healing cutoff behavior (i.e., Figure 3), implying that rate

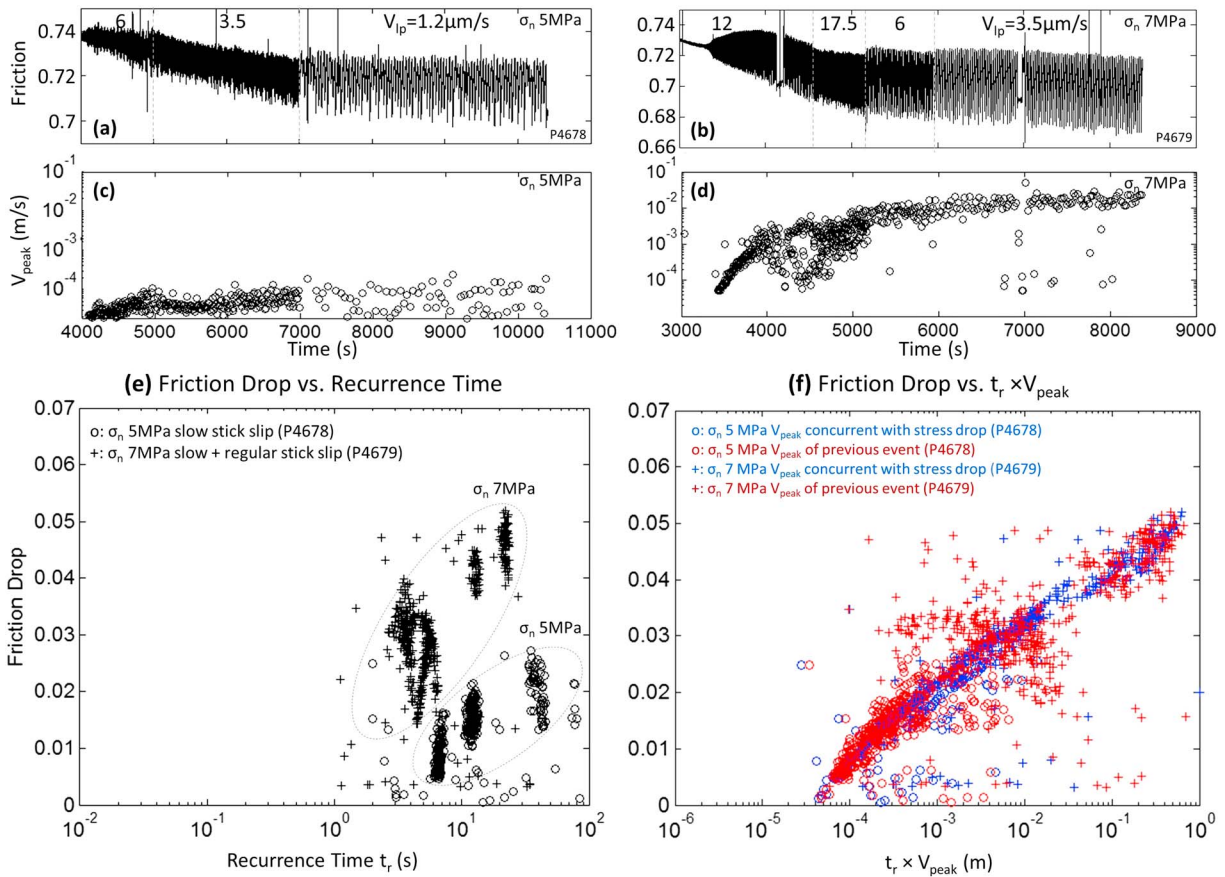


Figure 8. Lab data for friction versus time during repetitive stick-slip sliding at (a) 5 MPa and (b) 7 MPa cases. Loading velocities are given in each panel. (c and d) Peak slip velocity for each slip event. Note that V_{peak} is largest at 7 MPa and that it varies inversely with loading velocity, reflecting the result of greater inter-event frictional healing at lower loading rates. (e) Friction drop evolution with recurrence time for the two experiments, 5 MPa (circle) and 7 MPa (plus sign). Friction drop generally increases with t_r , although the scatter is large. (f) Friction drop versus $t_r \times V_{peak}$, using concurrent peak velocity (blue) and previous peak velocity (red).

and state healing governs the stick-slip evolution. This observation suggests that the cutoff time has an inverse relation to peak velocity and supports the prior numerical observation that cutoff time scales to the minimum value of the frictional state $\theta_i (=D_c/V_{peak})$.

Recurrence time is multiplied by the peak velocity of each slip event in Figure 8f to compensate for velocity variation effect. As discussed for Figures 7b, 7d, and 7f, if the cutoff time scales with D_c/V_{peak} , this will make the cutoff value dependent on D_c alone. Since the stick-slip is not perfectly periodic, velocities and friction drops vary within the same loading rate. We use peak velocities (V_{peak}) both (i) concurrent with the stress drop event (blue symbols) and (ii) from the previous slip event (red symbols). The velocity of the concurrent event is intrinsically related to the magnitude of the stress drop of the event while the velocity of the previous event may define the initial value of the frictional state and healing. In the numerical simulations, the two effects converge to a periodic stick-slip motion. Figure 8f strongly supports the internal mechanistic consistency of the numerical and theoretical explanations of stick-slip evolution. After multiplication of V_{peak} , the two trends for 5 MPa and 7 MPa converge with a single cutoff value. Using the concurrent velocity (blue) shows a distinct linear trend probably due to its intrinsic relation between slip velocity and stress drop. The trend with the previous velocity (red), albeit with some spread, also shows a clear linear trend overall. The scatter that appears at $t_r \times V_{peak} 10^{-3}$ – 10^{-2} m is significantly contributed by occasional nonperiodic stick-slip behavior, as observed by velocity variation in Figure 8c (7,000 s~) and Figure 8d (4,000–5,000 s). The scatter is strongly reduced in the other ranges that exhibit nearly periodic stick slips (as implemented in the numerical simulations). The back projected value to zero friction drop (a few tens of microns) is within a reasonable range for an appropriate D_c value of the gouge material used in this experiment (silica powder).

These observations imply that the periodicity (friction drop and recurrence) of laboratory stick-slip motion is strongly conditioned by D_c and V_{peak} , i.e., initial value of frictional state.

6. Conclusion

Rate and state frictional response defines frictional healing as a logarithm of the ratio between the initial frictional state (θ_i) and the evolution of this frictional state ($\theta_i + \Delta\theta$). The definition demonstrates an essential and prominent physical property of healing in that frictional strengthening is rapid on weakly healed surfaces (small θ_i) and conversely slow on strongly healed surface (high θ_i). Therefore, for the same change of frictional state ($\Delta\theta$), healing can be significant with a small initial state while it may be negligible at a large initial state. This property suggests that the magnitude of healing at a given time should be scaled to initial state θ_i . In typical slide-hold-slide experiments, θ_i is always regulated by D_c/V_{ip} . We show that in log linear healing, the cutoff time is scaled to D_c/V_{ip} .

As applied to earthquake faults, our results predict that higher earthquake slip velocity will cause a larger initial rate of frictional healing and therefore longer recurrence time with a given tectonic loading rate. Our novel continuous numerical solution of spring slider motion demonstrates that the cutoff recurrence interval in periodic stick-slip evolution also scales with frictional state at the conclusion of the dynamic slip process and that this frictional state can be evaluated from $\theta_i = D_c/V_{\text{peak}}$. Laboratory observations strongly support this explanation of evolution in friction drop. It is clearly shown that when peak velocity is slow, the evolution of friction drop is delayed.

Our results suggest that seismic hazard analysis based on the seismic cycle and earthquake periodicity should account for the frictional state at the conclusion of coseismic slip. We show that the magnitude of the anticipated earthquake event is conditioned by healing and modulated by antecedent behavior. Faster and larger healing follows after larger (lower frictional state due to higher peak slip velocity) events and consequently increased recurrence time are expected. The magnitude of the stress drop of the following slip event is determined by the amount of healing that occurs during this interseismic recurrence interval. These processes dictate earthquake periodicity. Both the earthquake magnitude (friction drop) and recurrence in repeating earthquakes are strongly conditioned by the (minimum) frictional state at the conclusion of dynamic friction drop.

Acknowledgments

We gratefully acknowledge the insights, suggestions and commentary from exceptionally thorough reviews by M. Ikari and A. Rubin. Data from numerical modeling are generated by the code available in the supporting information with all laboratory data available on request from the data repository hosted by Chris Marone at the Pennsylvania State University. This work is a partial result of support from the U.S. Department of Energy (DOE) under projects DE-EE0006761 and DE-FE0023354. This support is gratefully acknowledged.

References

- Bar-sinai, Y., Spatschek, R., Brenner, E. A., & Bouchbinder, E. (2014). On the velocity-strengthening behavior of dry friction. *Journal of Geophysical Research: Solid Earth*, *119*, 1738–1748. <https://doi.org/10.1002/2013JB010586>
- Baumberger, T., & Caroli, C. (2006). Solid friction from stick-slip down to pinning and aging. *Advances in Physics*, *55*(3–4), 279–348. <https://doi.org/10.1080/00018730600732186>
- Bayart, E., Rubin, A. M., & Marone, C. (2006). Evolution of fault friction following large velocity jumps. *Eos, Transactions of the American Geophysical Union*, *87*(52), Fall Meet. Suppl., Abstract S31A–0180.
- Beeler, N. M., Tullis, T. E., & Weeks, J. D. (1994). The roles of time and displacement in the evolution effect in rock friction. *Geophysical Research Letters*, *21*(18), 1987–1990. <https://doi.org/10.1029/94GL01599>
- Beeler, N. M., Hickman, S. H., & Wong, T. (2001). Earthquake stress drop and laboratory-inferred interseismic strength recovery. *Journal of Geophysical Research*, *106*(B12), 30,701–30,713. <https://doi.org/10.1029/2000JB900242>
- Beeler, N. M., Tullis, T., Junger, J., Kilgore, B., & Goldsby, D. (2014). Laboratory constraints on models of earthquake recurrence. *Journal of Geophysical Research: Solid Earth*, *119*, 8770–8791. <https://doi.org/10.1002/2014JB011184>
- Ben-david, O., Rubinstein, S. M., & Fineberg, J. (2010). Slip-stick and the evolution of frictional strength. *Nature*, *463*(7277), 76–79. <https://doi.org/10.1038/nature08676>
- Bhattacharya, P., Rubin, A. M., Bayart, E., Savage, H. M., & Marone, C. (2015). Critical evaluation of state evolution laws in rate and state friction: Fitting large velocity steps in simulated fault gouge with time-, slip-, and stress-dependent constitutive laws. *Journal of Geophysical Research: Solid Earth*, *120*, 6365–6385. <https://doi.org/10.1002/2015JB012437>
- Bhattacharya, P., Rubin, A. M., & Beeler, N. M. (2017). Does fault strengthening in laboratory rock friction experiments really depend primarily upon time and not slip? *Journal of Geophysical Research: Solid Earth*, *122*, 6389–6430. <https://doi.org/10.1002/2017JB013936>
- Blanpied, M. L., Marone, C. J., Lockner, D. A., Byerlee, J. D., & King, D. P. (1998). Quantitative measure of the variation in fault rheology due to fluid-rock interactions. *Journal of Geophysical Research*, *103*(B5), 9691–9712. <https://doi.org/10.1029/98JB00162>
- Brace, W. F., & Byerlee, J. D. (1966). Stick-slip as a mechanism for earthquakes. *Science*, *153*(3739), 990–992. <https://doi.org/10.1126/science.153.3739.990>
- Brechet, Y., & Estrin, Y. (1994). The effect of strain rate sensitivity on dynamic friction of metals. *Scripta Metallurgica et Materialia*, *30*(11), 1449–1454. [https://doi.org/10.1016/0956-716X\(94\)90244-5](https://doi.org/10.1016/0956-716X(94)90244-5)
- Carpenter, B. M., Scuderi, M. M., Collettini, C., & Marone, C. (2014). Frictional heterogeneities on carbonate-bearing normal faults: Insights from the Monte Maggio Fault, Italy. *Journal of Geophysical Research: Solid Earth*, *119*, 9062–9076. <https://doi.org/10.1002/2014JB011337>
- Chen, J., & Spiers, C. (2016). Rate and state frictional and healing behavior of carbonate fault gouge explained using microphysical model. *Journal of Geophysical Research: Solid Earth*, *121*, 8642–8665. <https://doi.org/10.1002/2016JB013470>

- Coulomb, C. A. (1785). Théorie des machines simples, en ayant égard au frottement de leurs parties, et à la roideur des cordages. *Memorie Mathematical Physics*, 161–342.
- Dieterich, J. I. (1972). Time-dependent friction in rocks. *Journal of Geophysical Research*, 77(20), 3690–3697. <https://doi.org/10.1029/JB077i020p03690>
- Dieterich, J. H. (1979). Modeling of rock friction: 1. Experimental results and constitutive equations. *Journal of Geophysical Research*, 84(9), 2161–2168.
- Dieterich, J., & Kilgore, B. (1994). Direct observation of frictional contacts: New insights for state-dependent properties. *Pageoph*, 143(1-3), 283–302. <https://doi.org/10.1007/BF00874332>
- Estrin, Y., & Brechet, Y. (1996). On a model of frictional sliding. *Pageoph*, 147(4), 745–762. <https://doi.org/10.1007/BF01089700>
- Frye, K. M., & Marone, C. (2002). Effect of humidity on granular friction at room temperature. *Journal of Geophysical Research*, 107(B11), ETG 11-1–ETG 11-13 2309. <https://doi.org/10.1029/2001JB000654>
- Giger, S. B., Cox, S. F., & Tenthorey, E. (2008). Slip localization and fault weakening as a consequence of fault gouge strengthening—Insights from laboratory experiments. *Earth and Planetary Science Letters*, 276(1-2), 73–84. <https://doi.org/10.1016/j.epsl.2008.09.004>
- Gu, Y., & Wong, T. (1991). Effects of loading velocity, stiffness, and inertia on the dynamics of a single degree of freedom spring-slider system. *Journal of Geophysical Research*, 96(B13), 21,677–21,691. <https://doi.org/10.1029/91JB02271>
- Gu, J.-C., Rice, J. R., Runia, A., & Tse, S. (1984). Slip motion and stability of a single degree of freedom elastic system with rate and state dependent friction. *Journal of the Mechanics and Physics of Solids*, 47(6), 1207–1218. [https://doi.org/10.1016/S0022-5096\(98\)00113-6](https://doi.org/10.1016/S0022-5096(98)00113-6)
- He, C., Wong, T., & Beeler, N. M. (2003). Scaling of stress drop with recurrence interval and loading velocity for laboratory-derived fault strength relations. *Journal of Geophysical Research*, 108(B1), 2037. <https://doi.org/10.1029/2002JB001890>
- Ikari, M. J., Marone, C., & Saffer, D. M. (2011). On the relation between fault strength and frictional stability. *Geology*, 39(1), 83–86. <https://doi.org/10.1130/G31416.1>
- Ikari, M. J., Carpenter, B. M., & Marone, C. (2016). A microphysical interpretation of rate- and state-dependent friction for fault gouge. *Geochemistry, Geophysics, Geosystems*, 17(5), 1660–1677. <https://doi.org/10.1002/2016GC006286>
- Ikari, M. J., Carpenter, B. M., Vogt, C., & Kopf, A. J. (2016). Elevated time-dependent strengthening rates observed in San Andreas Fault drilling samples. *Earth and Planetary Science Letters*, 450, 164–172. <https://doi.org/10.1016/j.epsl.2016.06.036>
- Johnson, T. L., & Scholz, C. H. (1976). Dynamic properties of stick-slip friction of rock. *Journal of Geophysical Research*, 81(5), 881–888. <https://doi.org/10.1029/JB081i005p00881>
- Karner, S., & Marone, C. (2000). Effects of loading rate and normal stress on stress drop and stick slip recurrence interval. In J. B. Rundle, et al. (Eds.), *Geocomplexity and the physics of earthquakes, Geophysical Monograph Series* (Vol. 120, pp. 187–198). Washington DC: American Geophysical Union. <https://doi.org/10.1029/GM120p0187>
- Karner, S. L., & Marone, C. (2001). Karner_Frictional restrengthening in simulated fault gouge: Effect of shear load perturbations. *Journal of Geophysical Research*, 106(B9), 19,319–19,337. <https://doi.org/10.1029/2001JB000263>
- Karner, S. L., Marone, C., & Evans, B. (1997). Laboratory study of fault healing and lithification in simulated fault gouge under hydrothermal conditions. *Tectonophysics*, 277(1-3), 41–55. [https://doi.org/10.1016/S0040-1951\(97\)00077-2](https://doi.org/10.1016/S0040-1951(97)00077-2)
- Leeman, J. R., Scuderi, M. M., Marone, C., Saffer, D. M., & Shinbrot, T. (2014). On the origin and evolution of electrical signals during frictional stick slip in sheared granular material. *Journal of Geophysical Research: Solid Earth*, 119, 4253–4268. <https://doi.org/10.1002/2013JB010793>
- Leeman, J. R., Saffer, D. M., Scuderi, M. M., & Marone, C. (2016). Laboratory observations of slow earthquakes and the spectrum of tectonic fault slip modes. *Nature Communications*, 7, 1–6. <https://doi.org/10.1038/ncomms11104>
- Linker, M. F., & Dieterich, J. H. (1992). Effects of variable normal stress on rock friction: Observations and constitutive equations. *Journal of Geophysical Research*, 97(B4), 4923–4940. <https://doi.org/10.1029/92JB00017>
- Mair, K., Frye, K. M., & Marone, C. (2002). Influence of grain characteristics on the friction of granular shear zones. *Journal of Geophysical Research*, 107(B10), 2219. <https://doi.org/10.1029/2001JB000516>
- Marone, C. (1998a). Laboratory-derived friction laws and their application to seismic faulting. *Annual Review of Earth and Planetary Sciences*, 26(1), 643–696. <https://doi.org/10.1146/annurev.earth.26.1.643>
- Marone, C. (1998b). The effect of loading rate on static friction and the rate of fault healing during the earthquake cycle. *Nature*, 391(6662), 69–72. <https://doi.org/10.1038/34157>
- Marone, C., & Saffer, D. M. (2015). *The mechanics of frictional healing and slip instability during the seismic cycle, Treatise on Geophysics* (2nd edn., pp. 111–138). Oxford, UK: Elsevier.
- Marone, C., Cocco, M., Richardson, E., & Tinti, E. (2009). The critical slip distance for seismic and aseismic fault zones of finite width. In E. Fukuyama (Ed.), *Fault-zone properties and earthquake rupture dynamics, International Geophysics Series* (Vol. 94, pp. 135–162). Burlington, MA: Elsevier.
- Mclasckey, G. C., Thomas, A. M., Glaser, S. D., & Nadeau, R. M. (2012). Fault healing promotes high-frequency earthquakes in laboratory experiments and on natural faults. *Nature*, 491(7422), 101–104. <https://doi.org/10.1038/nature11512>
- Nadeau, R. M., & Johnson, L. (1998). Seismological studies at Parkfield VI: Moment release rates and estimates of source parameters for small repeating earthquakes. *Bulletin of Seismological Society of America*, 88, 790–814.
- Nagata, K., Nakatani, M., & Yoshida, S. (2012). A revised rate- and state-dependent friction law obtained by constraining constitutive and evolution laws separately with laboratory data. *Journal of Geophysical Research*, 117, B02314. <https://doi.org/10.1029/2011JB008818>
- Nakatani, M., & Scholz, C. H. (2004). Frictional healing of quartz gouge under hydrothermal conditions: 1. Experimental evidence for solution transfer healing mechanism. *Journal of Geophysical Research*, 109, B07201. <https://doi.org/10.1029/2001JB001522>
- Nakatani, M., & Scholz, C. H. (2006). Intrinsic and apparent short-time limits for fault healing: Theory, observations, and implications for velocity-dependent friction. *Journal of Geophysical Research*, 111, B12208. <https://doi.org/10.1029/2005JB004096>
- Niemeijer, A., Marone, C., & Elsworth, D. (2008). Healing of simulated fault gouges aided by pressure solution: Results from rock analogue experiments. *Journal of Geophysical Research*, 113, B04204. <https://doi.org/10.1029/2007JB005376>
- Niemeijer, A. R., Boulton, C., Toy, V. G., Townend, J., & Sutherland, R. (2016). Large-displacement, hydrothermal frictional properties of DFDP-1 fault rocks, Alpine Fault, New Zealand: Implications for deep rupture propagation. *Journal of Geophysical Research: Solid Earth*, 121, 624–647. <https://doi.org/10.1002/2015JB012593>
- Perfettini, H., & Molinari, A. (2017). A micromechanical model of rate and state friction: 1. Static and dynamic sliding. *Journal of Geophysical Research: Solid Earth*, 122, 2590–2637. <https://doi.org/10.1002/2016JB013302>
- Rabinowicz, E. (1951). The nature of static and kinetic coefficients of friction. *Journal of Applied Physics*, 22(11), 1373–1379. <https://doi.org/10.1063/1.1699869>
- Rabinowicz, E. (1956). Stick and slip. *Scientific American*, 194(5), 109–119. <https://doi.org/10.1038/scientificamerican0556-109>

- Rathbun, A. P., & Marone, C. (2013). Symmetry and the critical slip distance in rate and state friction laws. *Journal of Geophysical Research*, *118*, 3728–3741. <https://doi.org/10.1002/jgrb.50224>
- Rice, J. R., & Ruina, A. L. (1983). Stability of steady frictional slipping. *Journal of Applied Mechanics*, *50*(2), 343–349. <https://doi.org/10.1115/1.3167042>
- Rice, J. R., & Tse, S. T. (1986). Dynamic motion of a single degree of freedom system following a rate and state dependent friction law. *Journal of Geophysical Research*, *91*(B1), 521–530. <https://doi.org/10.1029/JB091iB01p00521>
- Rice, J. R., Lapusta, N., & Ranjith, K. (2001). Rate and state dependent friction and the stability of sliding between elastically deformable solids. *Journal of the Mechanics and Physics of Solids*, *49*(9), 1865–1898. [https://doi.org/10.1016/S0022-5096\(01\)00042-4](https://doi.org/10.1016/S0022-5096(01)00042-4)
- Roy, M., & Marone, C. (1996). Earthquake nucleation on model faults with rate and state friction: Effects of inertia. *Journal of Geophysical Research*, *101*(B6), 13,919–13,932. <https://doi.org/10.1029/96JB00529>
- Rubinstein, J. L., Ellsworth, W. L., Chen, K. H., & Uchida, N. (2012). Fixed recurrence and slip models better predict earthquake behavior than the time- and slip-predictable models: 1. Repeating earthquakes. *Journal of Geophysical Research*, *117*, B02307. <https://doi.org/10.1029/2011JB008724>
- Ruina, A. (1983). Slip instability and state variable friction law. *Journal of Geophysical Research*, *88*(B12), 10,359–10,370. <https://doi.org/10.1029/JB088iB12p10359>
- Scholz, C. H. (1998). Earthquakes and friction laws. *Nature*, *391*(6662), 37–42. <https://doi.org/10.1038/34097>
- Scholz, C. H., & Engelder, J. T. (1976). The role of asperity indentation and ploughing in rock friction - I. *International Journal of Rock Mechanics and Mining Science and Geomechanics*, *13*(5), 149–154. [https://doi.org/10.1016/0148-9062\(76\)90819-6](https://doi.org/10.1016/0148-9062(76)90819-6)
- Scholz, C. H., Aviles, A., & Wesnousky, S. G. (1986). Scaling differences between large interplate and intraplate earthquakes. *Bulletin of the Seismological Society of America*, *76*, 65–70.
- Schwartz, D. P., & Coppersmith, K. J. (1984). Fault behavior and characteristic earthquakes: Examples from the Wasatch and San Andreas Fault Zones. *Journal of Geophysical Research*, *89*(B7), 5681–5698. <https://doi.org/10.1029/JB089iB07p05681>
- Scuderi, M. M., Carpenter, B. M., Johnson, P. A., & Marone, C. (2015). Poro mechanics of stick-slip frictional sliding and strength recovery on tectonic faults. *Journal of Geophysical Research*, *120*, 6895–6912. <https://doi.org/10.1002/2015JB011983>
- Scuderi, M. M., Marone, C., Tinti, E., Stefano, G. D., & Collettini, C. (2016). Precursory changes in seismic velocity for the spectrum of earthquake failure modes. *Nature Geoscience*, *9*(9), 695–700. <https://doi.org/10.1038/NGEO2775>
- Sleep, N. H. (2006). Real contacts and evolution laws for rate and state friction. *Geochemistry, Geophysics, Geosystems*, *7*(8), Q08012. <https://doi.org/10.1029/2005GC001187>
- Svetlizky, I., Bayart, E., Cohen, G., & Fineberg, J. (2017). Frictional resistance within the wake of frictional rupture fronts. *Physical Review Letters*, *118*(23), 1–5. <https://doi.org/10.1103/PhysRevLett.118.234301>
- Teng-Fong, W., & Yusheng, Z. (1990). Effects of load point velocity on frictional instability behavior. *Tectonophysics*, *175*(1–3), 177–195. [https://doi.org/10.1016/0040-1951\(90\)90137-W](https://doi.org/10.1016/0040-1951(90)90137-W)
- Tenthorey, E., & Cox, S. F. (2006). Cohesive strengthening of fault zones during the interseismic period: An experimental study. *Journal of Geophysical Research*, *111*, B09202. <https://doi.org/10.1029/2005JB004122>
- Vidale, J. E., Ellsworth, W. L., Cole, A., & Marone, C. (1994). Variations in rupture process with recurrence interval in a repeated small earthquake. *Nature*, *368*(6472), 624–626. <https://doi.org/10.1038/368624a0>
- Yasuhara, H., Marone, C., & Ellsworth, D. (2005). Fault zone restrengthening and frictional healing: The role of pressure solution. *Journal of Geophysical Research*, *110*, B06310. <https://doi.org/10.1029/2004JB003327>